Indian Journal of Pure & Applied Physics
Vol. 60, March 2022, pp. 274-282

Epoxy-based Light Weight Gamma Ray Shielding Materials

Shailesh Joshi[a, d], S Chandrasekaran[b], I Vijayalakshmi[a], K Sivasubramanian[a], V Jayaraman[c, d]

[a]Radiological & Environmental Safety Division, Indira Gandhi Centre for Atomic Research, Kalpakkam, India, 603 102

[b]Health & Industrial Safety Division, Indira Gandhi Centre for Atomic Research, Kalpakkam, India, 603 102

[c]Materials Chemistry Division, Indira Gandhi Centre for Atomic Research, Kalpakkam, India, 603 102

[d] Homi Bhabha National Institute, Mumbai, Maharashtra 400094

Received 13 August 2019; accepted 3 February 2022

Lightweight epoxy-based X-ray /gamma-ray shielding materials were synthesized by blending epoxy resin with the different weight percent of lead oxide, bismuth oxide, and tungsten oxide powders. The synthesized composites were characterized using FTIR, elemental analyzer, and X-ray radiography for their chemical structure, elemental composition, and filler distribution. The photon interaction parameters such as linear/mass attenuation coefficient, attenuation percentage, and half value layer were determined for all composites at photon energies 59.5, 364, and 661.7 keV. The measured mass attenuation coefficients of epoxy composites matched well with the obtained from XCOM. Moreover, the shielding effectiveness of the composites was analyzed by the half-value layer and heaviness of the composites and was compared with conventional shielding materials (concrete, lead, and steel).

Keywords: Composite, Shielding material, Linear attenuation coefficient, Half value layer

1 Introduction

Nuclear materials have established their worth in various industries, including nuclear power plants, medicine, agriculture, and electronics[1-5]. However, the handling of radioactive materials necessitates the proper shielding to minimize the exposure that otherwise may lead to catastrophic effects on society[6]. The prerequisite for the choice of shielding material depends primarily upon the type and energy of the radiation[7]. Moreover, as the X-rays/ Gamma rays interact with the electrons of the medium, it is highly desirable to design materials with high atomic numbers and high density to be enrolled as shielding materials for X/ Gamma rays[8-10].

In this scenario, lead is the best suitable shielding material for X-rays/ Gamma rays due to its high density and high atomic number (Z=82). However, it incurs various disadvantages associated due to its heaviness, toxicity, and poor chemical stability. This leads to the necessity of designing alternate shielding materials to overcome the problems posed by lead[8,11,12]. In this regard, different glass-based systems like oxides of lead, barium, and boron[13], lead oxide-silicon oxide-based glass[14], lead zinc borate glass[15], barium oxide- fly ash-based glass systems[16] are being employed as alternate shielding materials.

The glass-based materials have good radiation shielding properties but are expensive and brittle[17]. On the other hand, concrete and high-density concrete filled with hematite, magnetite, barium sulfate, steel scrap, and steel magnetite are also used as alternate shielding materials[18-23]. However, although these materials have good strength, they are inferior in compactness to metals and hence suffer the issue of more quantity required for the shielding. On the other hand, concrete is also used as a structural material in nuclear power plants and other radiation facilities containing ventilation ducts and pipes in straight or bent shapes through which the radiation streaming takes place [6,24]. To overcome the problem of radiation streaming, it is primarily required to construct irregular-shaped shielding, which becomes difficult to achieve using concrete or lead casting.

Recently polymer-based materials are being developed for shielding X-rays/ Gamma rays on account of their lightweight, easy processability, excellent mechanical properties, radiation and chemical stability, and feasibility to mold in irregular shapes[12, 17]. Various polymer composites (polyester, PVC rubber, polypyrrole, isophthalic resin, methyl vinyl silicone rubber, ethylene vinyl acetate,

*Corresponding author: (E-mail: shailesh@igcar.gov.in)

polydimethylsiloxane, styrene-butadiene rubber, and epoxy based) filled with lead and non-lead fillers (bismuth and tungsten) were developed for X-rays/ Gamma rays shielding[25-33, 12]. Among them, epoxy-based polymer composites are the materials of interest due to sound radiation and mechanical stability, facile preparation, and the availability of a wide range of unmodified epoxy resins and modifiers as starting materials[17,33,34]. Recently, several epoxy-based polymer composites have been developed as gamma-ray shielding materials (Table 1).

In this work, we attempted to develop a polymeric substitute of concrete that can be molded in irregular shapes and have better shielding properties than exhibited by the concrete for radiation streaming problems. Epoxy was used as polymer matrix, and fillers like lead oxide (lead-based), bismuth and tungsten oxide (lead-free) were used as fillers owing to their high atomic number and density. The work was carried out in two steps, where the first part describes the synthesis and characterization (Fourier transform infrared spectroscopy (FTIR), elemental analyzer, and X-ray radiography) of epoxy metal composites with 0-60 % filler contents. Subsequently, in the second part, the synthesized lead/lead-free epoxy metal composites were examined as shielding materials for X/ gamma rays by gamma attenuation studies. Shielding parameters like linear/mass attenuation coefficients, % attenuation, and half-value layer (HVL) of all composites were estimated at energy range 59.5 to 661.7 keV using ^{241}Am, ^{133}Ba, and ^{137}Cs radiation sources and planar High Purity Germanium (HPGe) detector and were compared with standard gamma shielding materials. In addition, the experimental values of mass attenuation coefficient at different energies were compared with XCOM values.

2 Materials and Methods

2.1 Materials

All starting chemicals used were of analytical grade. Araldite CY-205 (Huntsman) was used as unmodified epoxy resin, Jeffamine T-403 (Huntsman) served as amine-based modifier, Pb_3O_4, Bi_2O_3, and WO_3 (Loba Chemicals, India) were used as fillers in the composites.

Table 1 — Epoxy composites used as gamma shielding materials

Composites	Reference
Fe, Bi, Ta, WC/ epoxy composites	35
Tungsten borides/ epoxy micro-composites	36
Hafnium dioxide- and tungsten trioxide/ epoxy composites	37
Bi_2O_3 and WO_3/ epoxy micro and nano composites	38
Vanadium slag/Epoxy resin	39
Al_2O_3 and Fe_2O_3/ epoxy nanocomposites	40

2.2 Synthesis of Epoxy metal composites

The calculation of the desired amount of reactant was carried out using the concept of an equivalent weight of reacting groups (amine and epoxide) as mentioned in the literature[41]. Therefore, using amine hydrogen equivalent weight of amine and epoxide equivalent weight of epoxide, 43.6 g JeffamineT-403 was taken for the synthesis of 100 g of Araldite CY-205. The epoxy composites were synthesized using 0-60 wt% filler, and the amount of filler was calculated using equation 1.

$$Weight\ \% = \frac{weight\ of\ filler}{weight\ of\ filler + weight\ of\ polymer} * 100\ \% \quad \ldots(1)$$

Subsequently, a known amount of filler was uniformly mixed with the hardener (Jeffamine T-403) via a mechanical stirrer at 150 rpm for 60 minutes, followed by the addition of unmodified epoxy resin and stirring at 150 rpm for 60 minutes. The mixture was then degassed in a vacuum oven to avoid the formation of air bubbles and was poured in the polypropylene cylindrical mold (diameter 3 cm, height 1 cm) and kept overnight for curing. The synthesis of epoxy composites was carried out in triplicate.

2.3 Characterization

The density of epoxy composites was measured using ASTM D4142. Elementar make vario micro cube elemental analyzer was used for elemental analysis. FTIR spectra of the composites were recorded from 4000 to 500 cm^{-1} on an ABB-MB 3000 spectrometer, and spectra were analyzed using Horizon MB software. All measurements were carried out using 32 scans and 4 cm^{-1} resolution. The distribution of fillers in the polymer matrix was examined by X-ray radiography using Agfa D2 (100x300 mm) X-ray films and 75 kV X-ray from Balteau 160 kV equipment. The source film distance was fixed to 800 mm, and film was exposed for 90 seconds. The gamma-ray shielding behavior of the samples was carried out using ^{241}Am, ^{133}Ba, and ^{137}Cs gamma sources and the BSI Planar HPGe detector. The sensitive thickness and sensitive area of the HPGe detector were 15 mm and 450 mm^2, respectively, and had a resolution of 450 eV at 122

keV of ^{57}Co. The energy calibration of the detector was accomplished using ^{241}Am, ^{133}Ba, and ^{137}Cs standard gamma-ray point sources.

2.4 Attenuation Studies

In order to evaluate gamma shielding behavior of epoxy metal composites, ^{133}Ba, ^{241}Am, and ^{137}Cs sources were used, and the counts were recorded using a planar HpGe detector. Fig. 1 shows the schematic arrangement of the experimental setup used for gamma attenuation study[42].

The shielding studies were carried out by fixing sample dimensions (diameter: 3 cm and thickness: 1 cm) for all samples. The gamma-ray energy signatures of 59.5 keV of ^{241}Am, 356 keV of ^{133}Ba, and 661.7 keV of ^{137}Cs were employed in the study. Stainless steel collimator (OD=30 mm, ID=3 mm) was used before the detector and after the sample to get the narrow beam geometry. At first, the counts due to all energy peaks were measured in the respective geometric setup for 10 minutes. Later the epoxy discs were interposed between the source and detector surface one by one without disturbing the earlier arrangement. Each disc was examined three times and the average value was reported.

3 Results and discussions

3.1 Variation of density with weight fraction of fillers

Epoxy composites were prepared using Pb_3O_4, Bi_2O_3, and WO_3 fillers in 0-60 weight %. It was observed that an increase in the weight fraction of fillers from 0-60 wt % increased the density of composites from 1.10 ± 0.020 to 2.32 ± 0.040 g/cm^3 (Pb_3O_4 filled epoxy), 2.29 ± 0.030 g/cm^3 (Bi_2O_3 filled epoxy) and 2.20 ± 0.042 (WO_3 filled epoxy). For each composition, Pb_3O_4 filled composites had a slightly higher density than Bi_2O_3 and WO_3 filled composites Fig. 2 and can be attributed to the higher density of Pb_3O_4 (9.10 g/cm^3) as compared to Bi_2O_3 (8.90 g/cm^3) and WO_3 (7.16 g/cm^3).

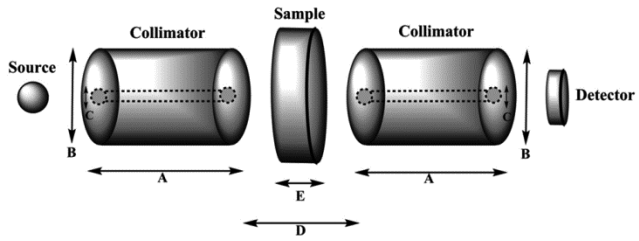

Fig. 1 — Geometric setup from narrow beam geometry from ^{241}Am, ^{133}Ba and ^{137}Cs sources[36], SS Collimator setup: A= 30 mm, B= 30 mm, C= 3 mm, D= 15 mm, E= 10 mm.

3.2 Infrared spectroscopic characterization of the composites

The IR spectrum of cured epoxy resin without fillers exhibits a broad peak at 3200 to 3600 cm^{-1} due to O-H stretching, the sharp absorption band at 1103 cm^{-1} due to C-N stretching vibration, absorption bands at 550 cm^{-1} due to N-H out of plane bending, benzene ring stretch at 1611 cm^{-1}, CH_3, CH_2 stretching and bending vibrations at 2864 cm^{-1}, 2982 cm^{-1} and 550 cm^{-1} respectively Fig. 3. Epoxide ring absorption peak at 910 cm^{-1} disappears in the composite, confirming the absence of any unreacted epoxy resin[43]. The FTIR spectra of 60% metal-loaded epoxy composites and pure epoxy Fig. 4 exhibit no appreciable change in the case of Pb_3O_4 as lead oxide mainly shows IR band below 400 cm^{-1}. However, a few very weak bands appear between 400 to 800 cm^{-1} due to impurities present in Pb_3O_4[44]. In the case of epoxy loaded with Bi_2O_3 a very weak peak appears at 629 cm^{-1} due to Bismuth oxide in addition to epoxy peaks[45]. In case of epoxy with 60 % WO_3, a broad peak appears in the

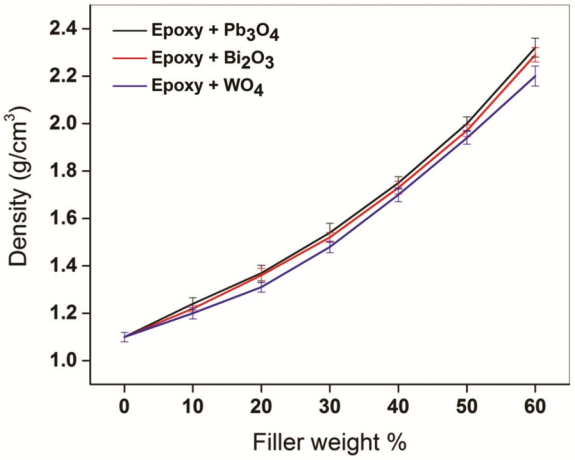

Fig. 2 — Density variations of composites with filler weight %.

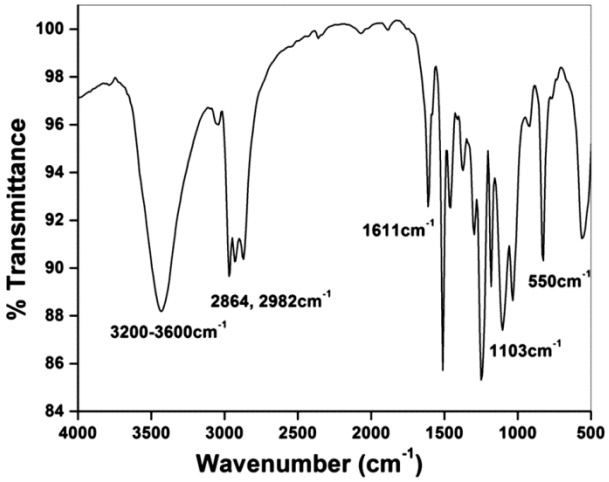

Fig. 3 — FTIR spectra of epoxy resin.

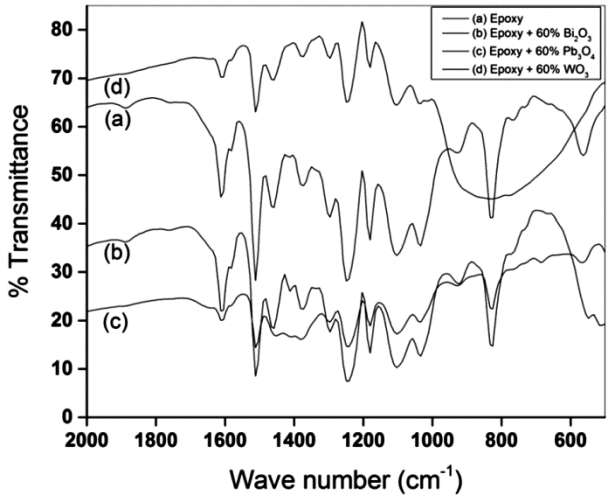

Fig.4 — FTIR spectra of epoxy composites (a) Epoxy (b) Epoxy+60 % Bi_2O_3 (c) Epoxy+60% Pb_3O_4 (d) Epoxy+60% WO_3.

range of 600 to 1000 cm^{-1} due to overlap of strong 832 cm^{-1} peak of epoxy and weak 731 and 835 cm^{-1} peaks of WO_3[46].

These findings imply that all composites exhibit epoxy peaks in addition to the filler peaks. Moreover, the absence of any new peak or disappearance of existing peaks is not occurring, which further indicates that shows no chemical reaction takes place between epoxy and metal oxides during composite formation.

3.3 Elemental Analysis

Effective atomic number (EAN) and electron density (ED) of epoxy-based composites were calculated by elemental composition and density of the composites using equations 2 and 3 (Tables 2-4)[47].

$$Z_{eff} = \sqrt[m]{\sum_j a_j}\, Z_j^m \quad \ldots(2)$$

where m = 2.94, a_j represents the fractional content of electrons belonging to the j^{th} constituent, Z_j is the atomic number of j^{th} constituent.

$$n_o = \rho N_A \sum_j \frac{w_j z_j}{A_j} \quad \ldots(3)$$

where n_o is the electron density (e/m^3), w_j is the fraction by weight, Z_j, A_j pertains to the atomic number and atomic weight of the j^{th} constituent. N_A Avogadro's constant and ρ is the density of the material in g/m^3.

It was observed that the EAN and ED of the composites show an increment upon increasing the filler weight % in all the cases. As expected, an increase in the filler weight % increases the Pb, Bi, and W weight percentage in the composites, thereby increasing the density of the composites. On account of the higher atomic number of these elements along with the higher density of composites (equations 4 and 5), an increment in the EAN and electron density was observed. It was observed that the Pb_3O_4 filled composites has slightly higher electron density as compared to other composites due to its high density (9.10 g/cm^3) and higher atomic number (82). Similarly Bi_2O_3 based composite has higher EAN due to its highest atomic number (83) among all three fillers.

Table 2 — Density, EAN and ED of Pb_3O_4 loaded epoxy matrix

Sample	Density (g/cm^3)	EAN	ED (e^-/m^3)
Epoxy	1.10 ± 0.020	6.23	3.66 x 10^{29}
Epoxy+10 % Pb_3O_4	1.24 ± 0.026	36.35	4.00 x 10^{29}
Epoxy+20 % Pb_3O_4	1.37 ± 0.033	45.89	4.33 x 10^{29}
Epoxy+30 % Pb_3O_4	1.54 ± 0.040	52.67	4.70 x 10^{29}
Epoxy+40 % Pb_3O_4	1.75 ± 0.027	58.07	5.21 x 10^{29}
Epoxy+50 % Pb_3O_4	2.00 ± 0.029	62.64	5.77 x 10^{29}
Epoxy+60 % Pb_3O_4	2.32 ± 0.040	66.65	6.49 x 10^{29}

Table 3 — Density, EAN and ED of Bi_2O_3 loaded epoxy matrix

Sample	Density (g/cm^3)	EAN	ED (e^-/m^3)
Epoxy	1.10 ± 0.020	6.23	3.66 x 10^{29}
Epoxy+10 % Bi_2O_3	1.22 ± 0.013	36.60	3.98 x 10^{29}
Epoxy+20 % Bi_2O_3	1.36 ± 0.030	46.29	4.25 x 10^{29}
Epoxy+30 % Bi_2O_3	1.52 ± 0.021	53.12	4.63 x 10^{29}
Epoxy+40 % Bi_2O_3	1.73 ± 0.027	58.58	5.15 x 10^{29}
Epoxy+50 % Bi_2O_3	1.97 ± 0.025	63.20	5.72 x 10^{29}
Epoxy+60 % Bi_2O_3	2.29 ± 0.030	67.23	6.41 x 10^{29}

Table 4 — Density, EAN and ED of WO_3 loaded epoxy matrix

Sample	Density (g/cm^3)	EAN	ED (e^-/m^3)
Epoxy	1.10 ± 0.020	6.23	3.66 x 10^{29}
Epoxy+10 % WO_3	1.20 ± 0.024	31.32	3.90 x 10^{29}
Epoxy+20 % WO_3	1.31 ± 0.021	39.60	4.15 x 10^{29}
Epoxy+30 % WO_3	1.48 ± 0.024	45.43	4.58 x 10^{29}
Epoxy+40 % WO_3	1.70 ± 0.030	50.09	5.12 x 10^{29}
Epoxy+50 % WO_3	1.94 ± 0.027	54.04	5.69 x 10^{29}
Epoxy+60 % WO_3	2.20 ± 0.042	57.49	6.30 x 10^{29}

3.4 X-ray radiography

The distribution of fillers in polymer matrix was estimated using X-ray radiography by exposing the pure epoxy and epoxy with 0-60 % Pb_3O_4 filled epoxy to 75 keV X-rays for 90 seconds, followed by analysis via digital X-ray images using ImageJ software[48] Figs. 5 (a-g) show the digital X-ray images of epoxy with different weight % of Pb_3O_4 (i) 0 % (ii) 10 % (iii) 20 % (iv) 30 % (v) 40 % (vi) 50 % (vii) 60 %,

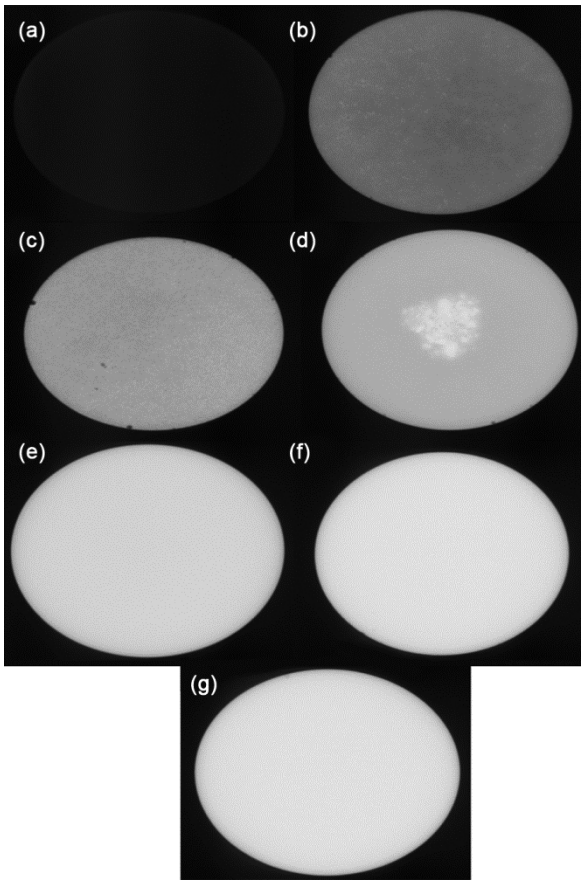

Fig. 5 — X-ray radiography digital images of epoxy with various % Pb_3O_4 (a) 0 % (b) 10 % (c) 20 % (d) 30 % (e) 40 % (f) 50 % (g) 60 %.

while Figs 6 (a-g) shows their corresponding intensity histograms. It was observed that in all cases, the intensity histogram shows unimodal characteristics, and most of the intensity values are within one standard deviation, thereby confirming the uniform distribution of the fillers in the polymer matrix for all composites. Furthermore, it was observed that as the filler content increases, the brightness of the images increases and gets saturated around 60 wt % filler content for 75 keV X-rays Figs. 5&7. This can be ascribed to the fact that an increase in the filler content leads to an elevation in Pb content, thereby augmenting the density of composites, which in turn leads to more X-rays getting attenuated, leading to brighter images Fig.6.

3.5 Gamma shielding studies

Gamma/X-ray photon interacts with the medium mainly by three modes (i) Photoelectric effect, (ii) Compton scattering, and (iii) Pair production. The probability of each interaction mainly depends upon the energy of the source and the chemical composition of the medium. Linear attenuation coefficient (μ) is the sum of the above three interaction probabilities and it depends upon the ratio of transmitted to the incident intensities and thickness of the medium[8, 28, 42].

$$\mu = -1/x \ln (I/I_0) \quad \ldots(4)$$

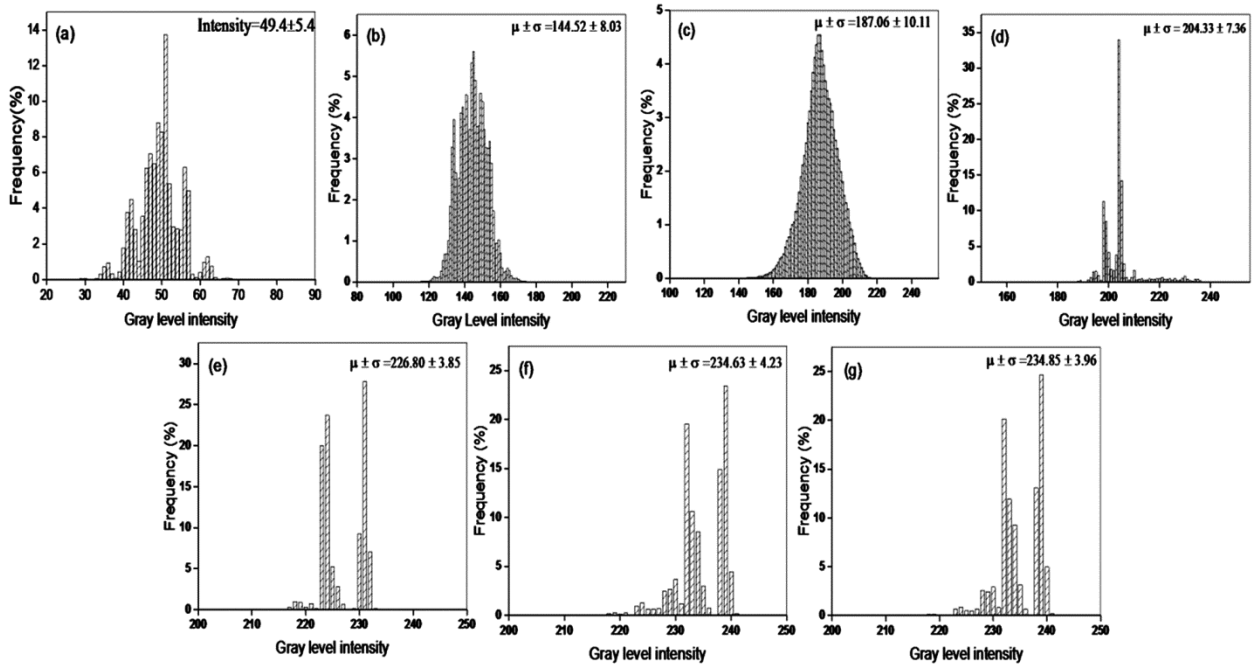

Fig. 6 — Intensity histogram of digital images of epoxy with varying % of Pb_3O_4 (a) 0 % (b) 10 % (c) 20 % (d) 30 % (e) 40 % (f) 50 % (g) 60 %.

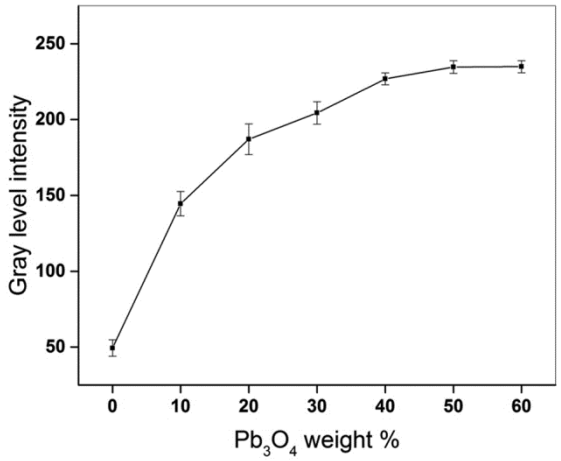

Fig. 7 — Gray level intensity variations with Pb_3O_4 weight %.

where I_0 and I are incident and transmitted photon intensity, x is the thickness (cm) of the medium, and μ is the linear attenuation coefficient (cm^{-1}) of the material. The amount of intensity is attenuated by the materials is represented by attenuation %, and can be calculated by equation 5[28, 42].

$$\% \text{ Attenuation} = (I_0 - I)/ I_0 * 100 \% \quad \ldots(5)$$

The half-value layer (HVL) and tenth value layer (TVL) represent the thickness of the material which will reduce the intensity of radiation to half and one-tenth, respectively and are given by equations 6 and 7[12, 28].

$$\text{HVL} = \ln 2/ \mu \quad \ldots(6)$$

$$\text{TVL} = 3.32 \text{ x HVL} \quad \ldots(7)$$

3.5.1 Effect of fillers on % attenuation

The experimental values of attenuation percentage of composites were calculated using equation 5, and it was observed that the attenuation percentage decreases with an increase in energy as the photoelectric effect dominates at lower gamma energies (<100 keV) Fig. 8(a). Epoxies loaded with 60 % Pb_3O_4 and Bi_2O_3 exhibit nearly same attenuation and are marginally higher than WO_3, which could possibly be due to higher atomic numbers of Pb and Bi as compared to W, in addition to the higher densities of Pb and Bi-based composites than W based ones. Further, variation of attenuation with filler content (Pb_3O_4) shows an increase with increasing filler weight % at all energies due to increment in high Z filler content and density of composites Fig. 8(b). It was also observed that the augmentation is higher at lower energy and gets

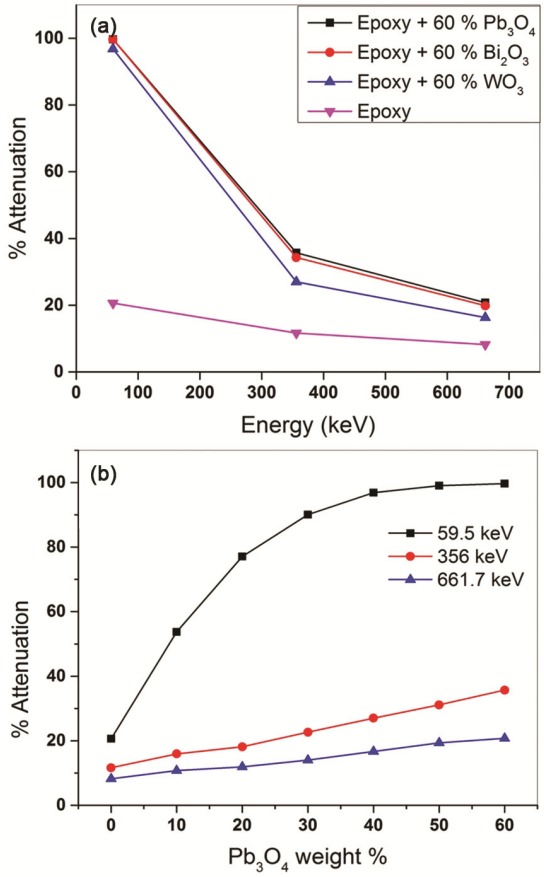

Fig. 8 — (a)Variation of % attenuation of epoxy composites with energy and (b) Variation of % attenuation of epoxy/ Pb_3O_4 composites with filler weight % at different energies.

saturated around 60 weight % at 59.5 keV due to photoelectric effect[25, 28]. Similar trend was observed in case of Bi and W loaded composites which showed an increase in % attenuation with filler weight %.

3.5.2 Effect of fillers on attenuation coefficient

Variation of linear attenuation coefficient (LAC) with energy and filler content shows a decrease in LAC with increasing energy, and the filled composites follow the order, $Pb_3O_4 > Bi_2O_3 > WO_3$ Fig. 9(a). It can be ascribed to the trend followed by these composites in terms of their densities and atomic number. It was observed that, the highest density of 60% Pb_3O_4 loaded composites (2.32 g/cm^3) with a higher atomic number of lead (82) shows higher LAC, on the other hand, 60 % WO_3 with the lowest density (2.22 g/cm^3) and lower atomic number (74) exhibits the least LAC. Further, for fixed energy, LAC increases with filler weight % and the increment is more prominent at lower energy (59.5 keV) as compared to high energy due to the fact that the photo

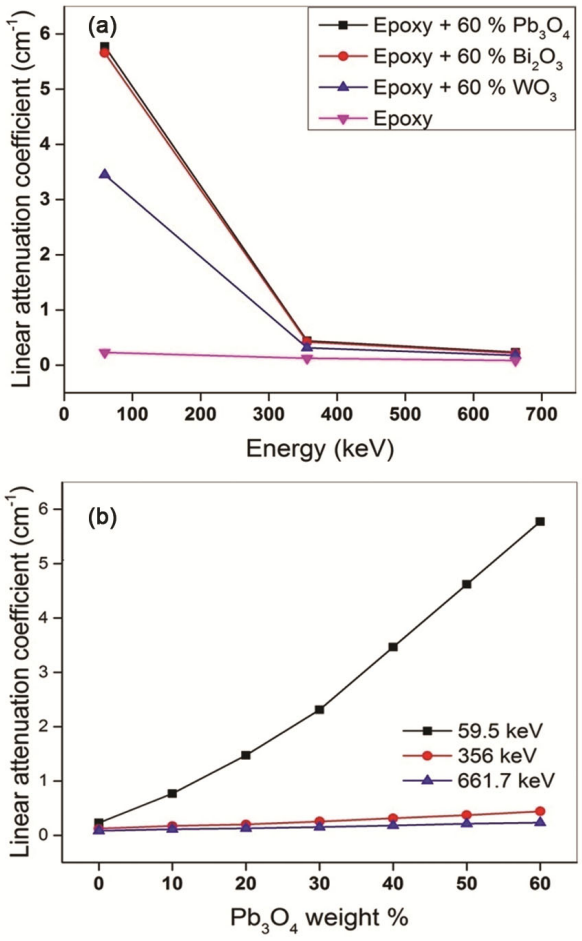

Fig. 9 — (a) Variation of linear attenuation coefficient of epoxy composites with gamma ray energy and (b) Variation of linear attenuation coefficient of epoxy/ Pb_3O_4 composites with filler weight % at different energies.

electric effect is the primary mode of interaction for low energy and high Z materials Fig. 9(b) [12, 28].

Further, the mass attenuation coefficient (μ/ρ) for epoxy composites was derived experimentally from their linear attenuation coefficient and density [Tables 5(a-c)]. Epoxy loaded with 60 % Pb_3O_4 has a maximum value of mass attenuation coefficient at all energies due to its highest density among all composites. In addition, the mass attenuation coefficient was also calculated by XCOM software[49] using elemental composition and density of composites, and the values are reported in parentheses in Tables 5(a-c). The mass attenuation coefficient values calculated by XCOM were compared with experimental values (Tables 5a-c), and a deviation of $< \pm 12$ % was observed between the measured and XCOM calculated values for all composites at all three energies (59.5, 356 and 661 keV).

Table 5(a) — Variations of mass attenuation coefficient of epoxy lead oxide composites, as a function of photon energy

Samples	Photon energy (keV)		
	59.5	356	661
	Mass attenuation coefficient in cm^2/g (XCOM value)		
Epoxy	0.210 (0.184)	0.112 (0.110)	0.077 (0.085)
Epoxy+10 % Pb_3O_4	0.621 (0.587)	0.140 (0.124)	0.092 (0.086)
Epoxy+20 % Pb_3O_4	1.070 (0.989)	0.146 (0.138)	0.092 (0.088)
Epoxy+30 % Pb_3O_4	1.510 (1.390)	0.167 (0.152)	0.098 (0.089)
Epoxy+40 % Pb_3O_4	1.980 (1.790)	0.180 (0.166)	0.104 (0.091)
Epoxy+50 % Pb_3O_4	2.310 (2.190)	0.186 (0.180)	0.107 (0.093)
Epoxy+60 % Pb_3O_4	2.490 (2.600)	0.190 (0.194)	0.100 (0.094)

Table 5(b) — Variation of mass attenuation coefficient of epoxy bismuth oxide composites, as a function of photon energy

Samples	Photon energy (keV)		
	59.5	356	661
	Mass attenuation coefficient in cm^2/g (XCOM value)		
Epoxy	0.210 (0.184)	0.112 (0.110)	0.077 (0.085)
Epoxy+10 % Bi_2O_3	0.593 (0.599)	0.139 (0.124)	0.090 (0.086)
Epoxy+20 % Bi_2O_3	1.020 (1.010)	0.143 (0.139)	0.093 (0.088)
Epoxy+30 % Bi_2O_3	1.495 (1.430)	0.155 (0.153)	0.092 (0.090)
Epoxy+40 % Bi_2O_3	1.872 (1.850)	0.175 (0.168)	0.099 (0.092)
Epoxy+50 % Bi_2O_3	2.258 (2.270)	0.186 (0.183)	0.106 (0.094)
Epoxy+60 % Bi_2O_3	2.470 (2.680)	0.189 (0.197)	0.094 (0.095)

Table 5(c) Variation of mass attenuation coefficient of epoxy tungsten oxide composites, as a function of photon energy

Samples	Photon energy (keV)		
	59.5	356	661
	Mass attenuation coefficient in cm^2/g (XCOM value)		
Epoxy	0.210 (0.184)	0.112 (0.110)	0.077 (0.085)
Epoxy+10 % WO_3	0.481 (0.436)	0.129 (0.118)	0.085 (0.086)
Epoxy+20 % WO_3	0.761 (0.688)	0.129 (0.126)	0.087 (0.086)
Epoxy+30 % WO_3	1.036 (0.940)	0.137 (0.134)	0.088 (0.086)
Epoxy+40 % WO_3	1.274 (1.193)	0.135 (0.143)	0.086 (0.087)
Epoxy+50 % WO_3	1.430 (1.440)	0.152 (0.151)	0.085 (0.087)
Epoxy+60 % WO_3	1.567 (1.690)	0.143 (0.159)	0.086 (0.087)

3.5.3 Effect of fillers on half value layer (HVL) and tenth value layer (TVL)

The HVL/TVL values for synthesized composites at different energies were calculated using equations 6 and 7 [Tables 6(a-c)]. A decrease in HVL/TVL was observed with increasing filler content at fixed energy. It is due to the fact that as filler content increases, the density of composites and content of

Table 6(a) — Effect of filler (Pb_3O_4) content on half value layer/Tenth value layer at different energies

Samples	Photon energy (keV)		
	59.5	356	661
	Half- value layer in cm (Tenth value layer)		
Epoxy	3.00 (9.96)	5.60 (18.59)	8.10 (26.89)
Epoxy+10 % Pb_3O_4	0.90 (2.98)	3.99 (13.24)	6.10 (20.25)
Epoxy+20 % Pb_3O_4	0.47 (1.56)	3.46 (11.48)	5.46 (18.12)
Epoxy+30 % Pb_3O_4	0.30 (0.99)	2.70 (8.96)	4.590 (15.24)
Epoxy+40 % Pb_3O_4	0.20 (0.66)	2.20 (7.30)	3.80 (12.62)
Epoxy+50 % Pb_3O_4	0.15 (0.49)	1.86 (6.17)	3.22 (10.69)
Epoxy+60 % Pb_3O_4	0.12 (0.39)	1.57 (5.21)	2.98 (9.89)

Table 6(b) — Effect of filler (Bi_2O_3) content on half value layer/Tenth value layer at different energies

Samples	Photon energy (keV)		
	59.5	356	661
	Half- value layer in cm (Tenth value layer)		
Epoxy	3.00 (9.96)	5.60 (18.59)	8.10 (26.89)
Epoxy+10 % Bi_2O_3	0.950 (3.15)	4.05 (13.44)	6.25 (20.75)
Epoxy+20 % Bi_2O_3	0.500 (1.66)	3.60 (11.95)	5.55 (18.42)
Epoxy+30 % Bi_2O_3	0.307 (1.02)	2.95 (9.79)	5.00 (16.60)
Epoxy+40 % Bi_2O_3	0.214 (0.71)	2.28 (7.56)	4.05 (13.44)
Epoxy+50 % Bi_2O_3	0.155 (0.51)	1.880 (6.24)	3.28 (10.88)
Epoxy+60 % Bi_2O_3	0.122 (0.40)	1.60 (5.31)	3.2 (10.62)

Table 6(c) — Effect of filler (WO_3) content on half value layer/Tenth value layer at different energies

Samples	Photon energy (keV)		
	59.5	356	661
	Half- value layer in cm (Tenth value layer)		
Epoxy	3.00 (9.96)	5.60 (18.59)	8.10 (26.89)
Epoxy+10 % WO_3	1.200 (3.98)	4.47 (14.85)	6.75 (22.41)
Epoxy+20 % WO_3	0.695 (2.30)	4.10 (13.61)	6.10 (20.25)
Epoxy+30 % WO_3	0.452 (1.50)	3.41 (11.32)	5.35 (17.76)
Epoxy+40 % WO_3	0.320 (1.06)	3.00 (9.96)	4.65 (15.44)
Epoxy+50 % WO_3	0.250 (0.830)	2.35 (7.80)	4.15 (13.77)
Epoxy+60 % WO_3	0.201 (0.667)	2.20 (7.30)	3.65 (12.12

high Z increases, leading to the ceasing of gamma rays more effectively, thereby decreasing HVL. Further, HVL decreases with an increase in energy for fixed filler content, and 60 % Pb_3O_4 loaded epoxy has the lowest HVL/TVL at 59.5 keV because a thicker sample is required to stop high energy gamma rays as compared to low energy. Epoxy composites filled with Pb_3O_4 and Bi_2O_3 had almost similar HVL for all energies due to their nearby atomic number and close density, whereas the WO_3 filled epoxy composite has slightly higher HVL on account of its lower atomic number and density as compared to lead and bismuth filled epoxy.

Table 7 — Comparison between epoxy composites and standard gamma shielding materials

Samples	Density (g/cm^3)	Photon energy (keV)		
		59.5	356	661
		Half- value layer in cm		
Epoxy	1.1	3	5.6	8.1
Epoxy+60 % Pb_3O_4	2.32	0.12	1.57	2.98
Epoxy+60 % Bi_2O_3	2.29	0.122	1.6	3.2
Epoxy+60 % WO_3	2.20	0.201	2.2	3.65
concrete	2.40	1.05	2.77	4.13
steel	7.80	0.13	0.83	1.3
lead	11.34	0.06	0.25	0.65

3.5.4 Comparison between epoxy composites and standard shielding materials

The shielding behavior of 60 % Pb_3O_4, Bi_2O_3, and WO_3 loaded epoxy composites was compared with standard shielding materials used for gamma rays e.g.; concrete, steel and lead (Table 7). Epoxy loaded with 60 % fillers show lower HVL values as compared to concrete at all three energies and also possesses a slightly lighter weight than concrete. It can be due to the high atomic number of fillers loaded in the epoxy matrix, which can stop gamma rays more effectively. Further epoxy composites with 60 % Pb_3O_4, Bi_2O_3 and WO_3 exhibit higher HVL values as compared to lead and steel. However, their weights are around one-third of steel and one-fifth of lead, which makes them a good candidate for irregular shape shielding for low energy gamma rays.

4 Conclusions

Epoxy-based lightweight X-ray/gamma-ray shielding materials were prepared using lead and non-lead (bismuth and tungsten-based) fillers in different weight % (0-60). The X-ray radiography studies of lightweight epoxies confirmed the uniform distribution of metal oxide in the polymer matrix. The experimental and calculated (XCOM) mass attenuation coefficients of shielding materials are closely matched. Moreover, 60 % filled epoxy composites display several advantages over standard concrete owing to their lower HVL/TVL values (energy range 59.5 to 667.1 keV), moldability for construction of irregular shaped configurations, and moderately lighter weights. These features make the lightweight epoxy composites (lead or non-lead) more desirable substitutes as a shielding material than concrete. In addition, they may also serve as lower

weight shielding substitutes for lead and steel for low energy X-/gamma rays.

Acknowledgment

The authors acknowledge Dr. B. Venkatraman, Director, Safety, Quality, and Resource Management Group, IGCAR, for his encouragement and support for carrying out the work presented in the paper. The authors acknowledge Mr. N Raghu for X-ray radiographic studies and Mr. Ajay Rawat for X-ray radiography image analysis.

References

1 Raj B, Mannan S L, Vasudeva Rao P R & Mathew M D, *Sadhana*, 27 (2007) 527.
2 Kowalsky R J & Perry J R, Radiopharmaceuticals in Nuclear Medicine Practice (Appleton and Lange, United States), 1987.
3 Anantharaman K, Shivakumar V & Saha D, *J Nucl Mater*, 383 (2008) 119.
4 Rodriguez P, *Bull Mat Sci*, 22 (1999), 215.
5 Toker C, Uzun B, Canci H & Ceylan F O, *Radiat Phys Chem,* 73 (2005), 365.
6 Martin J E, Physics for Radiation Protection: A Handbook. Wiley, Germany), 2nd Edn, 2006.
7 Glasstone S & Sesonske, Nuclear reactor engineering: reactor systems engineering. (Springer Science & Business Media, Dordrecht, 4th Edn, 2012.
8 Nambiar S & Yeow J T W, *Appl Mater Interfaces*, 4 (2012) 5717.
9 Kim J, Seo D, Lee B C, Seo Y S & Miller W H, *Adv Eng Mater*, 16 (2014) 1083.
10 Elmahroug Y, Tellili B & Souga C, *Ann Nucl Energy*, 75, (2015) 268.
11 McCaffrey J P, Shen H, Downton B & Hing E M, *Med Phys*, 34 (2007) 530.
12 Ambika M R, Nagaiah N & Suman S K, *J Appl Polym Sci*, 134 (2017) 44657.
13 Singh N, Singh K J, Singh K & Singh H, *Radiat Meas*, 41 (2006) 84.
14 Singh K J, Singh N, Kaundal R S & Singh K, *Nucl Instr Meth Phys Res B*, 266 (2008) 944.
15 El-Kamees S Y, El-Ghany S, El-Hakam Hazzoz M A & El-Gammam Y A A, *World J Condens Matter Phys* 3 (2013) 198.
16 Suparat T, Kaewkhao J, Limsuwan P & Chewpraditkul W, *Prog Nucl Sci Technol*, 1(2011) 110.
17 Noor Azman N Z, Siddiqui S A & Low I M, *Appl Phys A Mater Sci Process*, 110 (2013) 137.
18 Maghrabi H A , Vijayan A, Deb P & Wang L, *Text Res J*, 86 (2015) 649.
19 Waly E S A & Bourham M A, *Ann Nucl Energy*, 85 (2015) 306.
20 Kaur U, Sharma J K, Singh P S & Singh T, *Appl Radiat Isot*, 70 (2012) 233.
21 Bashter I I, El-Sayed Abdo A & Samir Abdel-Azim M, *Jpn J Appl Phys*, 36 (1997) 3692
22 Harish V, Nagaiah N, Prabhu T N & Varughese K T, *J Appl Polym Sci*, 112 (2009) 1503.
23 Gencel O, Bozkurt A, Kam E & Korkut T, *Ann Nucl Energy*, 38 (2011) 2719.
24 Shin K, *J Nucl Sci Technol* 26 (1989) 1067.
25 Nambiar S, Osei E K & Yeow J T W, *J Appl Polym Sci*, 127 (2012) 4939.
26 McCaffrey J P, Mainegra-Hing E & Shen H, *Med Phys*, 36 (2009) 5586.
27 Eid Gh A, Kany A I, El-Toony M M, Bashter I I & Gaber F A, *Arab J Nucl Sci Appl*, 46 (2013) 226.
28 Seyed S H Ezzati S N & Askari M, *Polym Adv Technol* 26 (2014) 561.
29 Harish V, Nagaiah N, Prabhu T N & Varughese K T, *Indian J Pure Appl Phys,* 50 (2012) 847.
30 Chai H, Tang X, Ni M, Chen F, Zhang Y, Chen D & Qiu Y, *J Appl Polym Sci*, 133 (2015) 43012.
31 Soylu M, Lambrecht F Y & Ersoz O A, *J Radioanal Nucl Chem*, 305 (2015) 529.
32 Li R, Gu Y, Wang Y, Yang Z, Li M & Zhang Z, *Mater Res Express* 4 (2017) 035035.
33 Noor Azman N Z, Siddique S A, Hart R & Low I M, *Appl Radiat Isot*, 71 (2013) 62.
34 Chang L, Zhang Y, Liu J, Fang J, Luan W, Yang X & Zhang W, *Nucl Instrum Methods Phys Res B*, 356 (2015) 88.
35 Canel A, Korkut H & Korkut T, *Radiat Phys Chem*, 158 (2019) 13.
36 Al Hassan M, Wang Z, Liu W B, Wang J, Zhigang Y, Khan M, Ali M M, Geldiyev R, Diaby M & Derradji M, *Radiat Phys Chem*, 158 (2021) 109769.
37 Higgins M C M, Radcliffe N A, Toro-González M & Rojas J V, *J Radioanal Nucl Chem*, 322 (2019) 707.
38 Karabul Y & İçelli O, *Results Phys*, 26 (2021) 104423
39 Dong M, Xue X, Yang H, Liu D, Wang C & Li Z, *J Hazard Mater*, 318 (2016) 751
40 Aldhuhaibat M J, Amana M S, Jubier N J & Salim A A, *Neuro Quantol*, 19 (2021) 79.
41 Burton B, Alexander D, Klein H, Vasquez A G, Pekarik A & Henkee C, Epoxy formulations using Jeffamine polyetheramines. (The woodlands, TX: Huntsman Corp), (2005)1.
42 Joshi S, Rao J S B , Sivasubramanian K, Kumar R, Jayaraman V & Venkatraman B, *J Polym Res*, 24 (2017) 78.
43 Gonzalez M G, Cabanelas J C & Baselga J, Infrared Spectroscopy- Materials Science, Engineering and Technology, 13 (2012), 261.
44 Salagram M, Prasad V K & Subrahmanyam K, *J Alloys Compd*, 335 (2002) 228.
45 Refat M S & Adam A M A, *Res Rev J Mat Sci*, 2 (2014) 1.
46 Manciu F S, Enriquez J L, Durrer W G, Yun Y, Ramana C V & Gullapalli S K, *J Mat Res*, 25 (2010) 2401.
47 Traub R J, Olsen P C & Mcdonald J C, *Radiat Prot Dosim*, 121 (2006) 202.
48 Schneider C A, Rasband W S & Eliceiri KW, *Nat Methods*, 9 (2012) 671.
49 Gerward L, Guilbert N, Jensen K B & Levring H, *Radiat Phys Chem*, 60 (2001) 23.